Research Square

Preprints are preliminary reports that have not undergone peer review.
They should not be considered conclusive, used to inform clinical practice,
or referenced by the media as validated information.

Mapper-based topological subtyping of early diuretic response in ICU patients with acute heart failure: a retrospective cohort study with external validation in eICU-CRD

Jiacheng Tian

tianjiacheng1918@gmail.com

Research Article

Keywords: acute heart failure, diuretic resistance, urine output, topological data analysis, Mapper, MIMIC-IV

Posted Date: March 10th, 2026

DOI: https://doi.org/10.21203/rs.3.rs-9012160/v1

License: This work is licensed under a Creative Commons Attribution 4.0 International License.
Read Full License

Additional Declarations: No competing interests reported.

Mapper-based topological subtyping of early diuretic response in ICU patients with acute heart failure: a retrospective cohort study with external validation in eICU-CRD

Jiacheng Tian[1*]

[1*]School of Nursing, Zunyi Medical University, Zunyi, Guizhou, 563000, China.

Corresponding author(s). E-mail(s): tainjiacheng1918@gmail.com;

Abstract

Purpose: Fixed-threshold definitions of diuretic resistance may miss heterogeneous and time-varying response patterns in ICU acute heart failure (AHF). We aimed to identify stable and interpretable subtypes of early loop-diuretic response using a Mapper-based topological framework with external validation.

Methods: In MIMIC-IV v3.1, we included adult ICU stays with an AHF diagnosis and first intravenous loop diuretic within 24 h of ICU admission (t_0). t_0-anchored features captured furosemide-equivalent exposure, cumulative urine output and diuretic efficiency index (DEI) over 2 h/6 h/12 h, and hemodynamic/renal context. Mapper graphs were built with two-stage parameter search and evaluated by bootstrap co-membership Jaccard similarity (200 iterations; 80% resampling). Branch labels were assessed for incremental prognostic value for in-hospital mortality using Cox and logistic regression, and for AKI within 48 h (KDIGO creatinine proxy) as a mechanistic endpoint. We performed external validation in eICU-CRD v2.0 using a harmonized pipeline.

Results: The cohort comprised 2,373 ICU stays. The optimal Mapper yielded 58 nodes and 393 edges (coverage 1.000) with high stability (mean Jaccard $\mathbf{0.924 \pm 0.038}$; stability score 0.944). Four major branches (A–D) showed marked mortality differences (log-rank $\boldsymbol{p = 1.659 \times 10^{-19}}$). After adjustment, branches C and D had higher mortality risk than A and improved discrimination (AUC 0.712 to 0.737). AKI48h also differed across branches ($\boldsymbol{p = 2.137 \times 10^{-7}}$). In eICU-CRD v2.0, the external validation recapitulated a comparable topology and major-branch structure with a consistent mortality-risk gradient (log-rank $\boldsymbol{p = 5.441 \times 10^{-4}}$).

Conclusion: t_0-anchored Mapper subphenotyping provides a stable and interpretable representation of diuretic-response heterogeneity in ICU AHF with independent prognostic and mechanistic relevance.

Keywords: acute heart failure, diuretic resistance, urine output, topological data analysis, Mapper, MIMIC-IV

1 Introduction

Acute heart failure (AHF) in critically ill patients is frequently accompanied by volume overload and impaired organ perfusion. Intravenous loop diuretics (e.g., furosemide) remain the cornerstone of early decongestion [1], but an impaired response—often described clinically as *diuretic resistance*—is common and associated with adverse outcomes [2].

Quantifying "response" by a fixed urine-output threshold within a short time window (e.g., urine output in the first 2 h) can be misleading in the ICU, where the observed urine output is strongly influenced by **time structure** (delayed response vs. true nonresponse), **patient context** (renal function, hemodynamics, and congestion), and **measurement sparsity** (missing records and catheter irrigation artifacts). As a result, threshold-based rules may under-recognize heterogeneous response phenotypes and fail to identify high-risk subtypes that appear similar early but diverge later.

Recent work has emphasized early quantitative response metrics such as diuretic efficiency and natriuresis/urinary sodium to guide decongestion and timely escalation, including diuretic potentiation and combination strategies [3–6]. However, ICU-specific response phenotypes can remain difficult to capture because the exposure–response relationship is time-varying and strongly confounded by baseline renal function, hemodynamics, and documentation patterns.

Unsupervised electronic health record phenotyping has been applied to characterize heterogeneity among cardiac intensive care unit patients with heart failure [7], motivating methods that are both robust and interpretable for bedside translation.

Topological data analysis (TDA) provides a global representation of complex data by focusing on the *shape* of the data manifold. Mapper compresses high-dimensional phenotypes into a network skeleton consisting of nodes (local clusters) and edges (overlaps), facilitating visual exploration and interpretable "branch annotation" by projecting clinical features and outcomes onto network structure [8–10]. Compared with black-box risk models that output only a scalar score, Mapper can yield an explicit response "spectrum" that is easier to interpret clinically.

We therefore developed a standardized ICU AHF workflow to characterize early loop-diuretic exposure–response–context patterns and to identify stable subtypes using Mapper. We anchored feature construction at the first intravenous loop-diuretic dose time (t_0), derived short-window cumulative urine output and a diuretic efficiency index (DEI), integrated hemodynamic and renal context, and built Mapper graphs with parameter search and bootstrap stability quantification. We then examined whether Mapper-derived branches provide independent and incremental prognostic information for in-hospital mortality beyond conventional covariates. To strengthen the mechanistic chain, we additionally assessed acute kidney injury within 48 h after $t_0$using a KDIGO creatinine-based proxy, and we prespecified sensitivity analyses to address DEI denominator artifacts and bias from highly missing monitoring variables (central venous pressure, CVP).

2 Materials and methods

2.1 Data source

We used the de-identified MIMIC-IV v3.1 database as the derivation cohort [11] and the eICU Collaborative Research Database (eICU-CRD) v2.0 as the external validation cohort [12, 13]. Both are publicly available via PhysioNet to credentialed users who complete the required training and data use agreements.

2.2 Study cohort

The unit of analysis was the ICU stay (`icu.icustays`). Inclusion criteria were: **(1)** age $\geq$ 18 years; **(2)** an ICD-9 diagnosis consistent with acute heart failure; and **(3)** at least one eligible intravenous loop-diuretic administration within 24 h of ICU admission. The first eligible administration time was defined as the treatment anchor t_0. We excluded patients with ICD-9 evidence of end-stage kidney disease or dialysis (ESRD/dialysis) and those with sepsis.

To reduce manual hard-coding, we generated the ICD-9 code set by keyword matching against diagnosis descriptions (`hosp.d_icd_diagnoses.long_title`) and used the resulting code list for cohort construction.

2.3 External validation cohort and analysis framework (eICU-CRD v2.0)

We performed external validation using the eICU-CRD v2.0 cohort by aligning the phenotyping pipeline with the main MIMIC-IV analysis, including t_0-anchored feature extraction, harmonized feature definitions, Mapper modeling, and

the same outcome-analysis framework (Supplementary Material). Because precise event timestamps were not uniformly available in eICU-CRD, time-to-event analyses used length of stay as a proxy time scale.

2.4 $t_0$anchor and time windows

ICU admission time was `intime`. The diuretic anchor $t_0$was defined as the first qualifying intravenous loop-diuretic administration within 24 h of `intime`. With respect to t_0, we defined urine-output response windows of 0–2 h, 0–6 h, and 0–12 h; a vital-sign baseline window of t_0-6 h to t_0+2 h; and a laboratory baseline window of t_0-24 h to t_0+6 h.

2.5 Variables and preprocessing

Unless otherwise specified, detailed variable/item definitions, code lists, and additional implementation details are provided in the Supplementary Material.

2.5.1 Exposure: intravenous loop-diuretic dose

We extracted intravenous loop-diuretic administrations from `icu.inputevents`, including furosemide (itemid 221794, 228340) and bumetanide (itemid 229639). We kept records with `amountuom=mg` and excluded implausible entries (`amount`$\leq$ 0 or $>$ 5000). Doses were converted to furosemide equivalents (furosemide $\times$1; bumetanide $\times$40). We constructed: `first_dose_furosemide_eq_mg`, `furosemide_eq_total_24h_mg`, `diuretic_events_n_24h`, and `minutes_icu_to_first_diuretic`.

2.5.2 Response: cumulative urine output and DEI after t_0

We extracted urine-output records from `icu.outputevents`, restricted to `valueuom=mL` and $0 \leq$ `value` ≤ 5000. Mixed "urine/irrigation output" items (226566, 227489) and pure urine-output items were treated as positive; genitourinary irrigation input (227488) was treated as negative to compute net urine output. We computed cumulative net urine output for 0–2 h, 0–6 h, and 0–12 h, and truncated the cumulative value at 0 to avoid non-physiologic negative urine output:

$$UO_{0\text{–}T} = \max\Big(\sum_{t\in[0,T]} \text{adjusted_urine}(t),\, 0\Big),$$
$$T \in \{2\,\text{h},\, 6\,\text{h},\, 12\,\text{h}\}.$$

The diuretic efficiency index (DEI) was defined as urine output per dose (mL/mg). We retained both an observed version (preserving missingness) and a zero-filled version for sensitivity analyses that probe the assumption "not recorded implies no measured output".

Table 1: Missingness of key variables ($n = 2373$).

Variable	Missing (n)	Missing (%)
Urine output missing (12 h)	23	0.97
DEI missing (6 h)	23	0.97
MAP nearest value missing	15	0.63
Baseline creatinine missing	130	5.48
CVP nearest value missing	1,914	80.66
Baseline NT-proBNP missing	2,081	87.69

2.5.3 Hemodynamics and laboratory baselines

Mean arterial pressure (MAP) was extracted from invasive/non-invasive MAP (itemid 220052, 220181), restricted to 20 mmHg–200 mmHg. CVP (itemid 220074) was restricted to -5 mmHg–35 mmHg. Within the t_0-6 h to t_0+2 h window, we extracted the nearest value to $t_0$and the window median. Laboratory values (creatinine, blood urea nitrogen (BUN), sodium, NT-proBNP) were extracted as the nearest measurement within t_0-24 h to t_0+6 h, with physiologic-range filters.

2.5.4 Mapper feature set and scaling

We used 16 features for Mapper (urine output/DEI, dose, time-to-dose, MAP, CVP, creatinine, BUN, sodium, age, and a CVP-missingness indicator). For right-skewed non-negative variables (dose, urine output, DEI, time-to-dose, BUN), we applied a $\log(1+x)$ transformation, followed by robust scaling (`RobustScaler`). To avoid selection bias due to missingness, we imputed numeric missing values in the Mapper feature matrix using multiple imputation by chained

equations (MICE; $m = 20$, max_iter=20) [14]. In contrast, the downstream Cox/logistic models used median imputation for the core covariates (age, baseline creatinine, MAP, and 24 h total dose) to keep models parsimonious.

2.6 Mapper modeling, parameter selection, and stability

2.6.1 Mapper construction

We used the Giotto-TDA implementation of Mapper. Candidate lenses (filters) were: two-dimensional PCA (`pca2d`), a two-dimensional projection of DEI_6h and baseline creatinine (`dei_creatinine_2d`), and DEI_6h with CVP (`dei_cvp_2d`). We used `CubicalCover` for the cover and DBSCAN for local clustering [15].

Parameter selection used two stages: a coarse grid search ($n_intervals \in \{10, 12, 14\}$, $overlap_frac \in \{0.25, 0.35, 0.45\}$, $\varepsilon \in \{0.8, 1.0, 1.2\}$, and `min_samples`$\in \{5, 8\}$; 162 combinations), followed by local refinement around high-scoring regions with denser candidate values.

2.6.2 Stability evaluation and final selection

We first screened candidates using structural quality diagnostics (coverage, node-size behavior, and connectivity/branching), and then quantified stability via bootstrapping: 200 iterations with 80% resampling without replacement. For each bootstrap graph, we compared patient-pair co-membership relations with the full-sample graph and computed the Jaccard similarity. We combined the mean Jaccard with penalties for variability in node counts/structure to obtain a stability score and selected the parameter set optimizing stability and structural quality (Table 2).

2.7 Branch definition and clinical annotation

We aggregated node-level communities and labeled major branches ($\geq$ 20 stays) as A–D; sparse small branches were retained but grouped as Minor in summaries. Branch annotation used medians/proportions of key features and outcomes (e.g., DEI, creatinine, sodium, CVP, and in-hospital mortality).

Table 2: Optimal Mapper parameters and graph statistics (full cohort).

Metric	Value
Lens	`pca2d`
$n_intervals$	8
$overlap_frac$	0.55
DBSCAN ε	0.7
DBSCAN `min_samples`	8
Nodes / edges	58 / 393
Coverage	1.000
Largest connected component ratio	1.000
Number of connected components	1
Modularity	0.399
Bootstrap Jaccard (mean±SD)	0.924 ± 0.038
Stability score	0.944
Final score	0.859

2.8 Outcomes and statistical analysis

2.8.1 Primary outcome: in-hospital mortality

The primary outcome was in-hospital mortality (`hospital_expire_flag`). Time-to-event was measured from $t_0$to death time (`deathtime`) or discharge (`dischtime`). We constructed Kaplan–Meier curves and compared branches using the multi-group log-rank test. Multivariable Cox regression and logistic regression evaluated the independent prognostic value of branches, adjusting for age, sex, baseline creatinine, nearest MAP, and 24 h total furosemide-equivalent dose (`log_dose24`). Incremental value was assessed via likelihood-ratio tests and changes in C-index/AUC.

2.8.2 Secondary outcome: AKI within 48 h (KDIGO creatinine proxy)

To strengthen the mechanistic chain (diuretic response $\rightarrow$ kidney injury $\rightarrow$ prognosis), we defined AKI within 48 h after $t_0$using a KDIGO creatinine-based proxy [16]. Baseline creatinine was the nearest measurement within t_0-24 h to t_0+6 h. Follow-up creatinine was the maximum value within $t_0$to t_0+48 h. AKI48h was defined as either $\Delta\mathrm{Cr} \geq 0.3$ mg/dL or $\mathrm{Cr}_{48h,\max} \geq 1.5 \times \mathrm{Cr}_{baseline}$. Stage 2+ (severe AKI) was defined as $\mathrm{Cr}_{48h,\max} \geq 2.0 \times \mathrm{Cr}_{baseline}$. Because urine-output response was part of the feature set, we did

not include the KDIGO urine-output criterion to avoid outcome–feature overlap.

2.8.3 Sensitivity analyses: DEI denominator artifacts and high CVP missingness

We prespecified sensitivity analyses to address (i) denominator artifacts in DEI driven by extremely small recorded doses, and (ii) structural bias introduced by highly missing monitoring variables (CVP/NT-proBNP). DEI robustness scenarios included a dose floor (10 mg), excluding stays with first dose < 5 mg, and replacing the first-dose denominator with the 24 h total dose. We also repeated Mapper construction with CVP fully removed (and no missingness indicator) versus retained with a missingness indicator, and we compared observed versus zero-filled response variables.

3 Results

3.1 Cohort characteristics and missingness

We included 2,373 ICU stays (Table 3). Missingness of urine-output/DEI features and MAP was below 1%, suggesting relatively complete short-window urine-output recording around $t_0$in ICU. Baseline creatinine had 5.48% missingness. In contrast, CVP and NT-proBNP were highly sparse (80.66% and 87.69% missing), motivating explicit missingness handling and sensitivity analyses (Table 1).

3.2 Mapper graph and major branches

The optimal Mapper graph is shown in Figure 1. The graph achieved full coverage (1.000), contained 58 nodes and 393 edges, and formed a single connected component (largest-component ratio 1.000) with modularity 0.399. Bootstrap co-membership analysis yielded a mean Jaccard similarity of 0.924 ± 0.038 and a stability score of 0.944, indicating a robust network skeleton.

Branch summaries are shown in Table 4. Branch A was the largest ($n = 1747$) and exhibited higher DEI and lower kidney-injury burden, consistent with a more typical "responsive" spectrum. Branch B ($n = 461$) showed intermediate DEI but substantially higher 24 h dose, suggesting a transition state with dose escalation and heterogeneous response. Branch C ($n = 105$) had very low DEI with higher creatinine/BUN and one of the highest mortality rates, consistent with severe cardiorenal syndrome/true resistance. Branch D ($n = 60$) had DEI-6h median of 0 and enrichment of a primary nonresponse pattern, suggesting an early nonresponse or delayed-response pathway.

3.3 Outcome associations: unadjusted and adjusted evidence

Kaplan–Meier curves and the log-rank test showed significant survival heterogeneity across branches (Figure 2; $p = 1.659 \times 10^{-19}$). After adjustment for age, sex, baseline creatinine, MAP, and 24 h total dose, adding branch labels significantly improved the Cox model fit (LRT $p = 2.362 \times 10^{-8}$) and discrimination (C-index 0.716 to 0.756). Compared with branch A, branches C and D had substantially higher mortality risk (HR 2.27 and 4.27), whereas branch B had an adjusted HR of 0.79 (not statistically significant).

Logistic regression for in-hospital mortality yielded concordant findings: adding branches improved model fit (LRT $p = 1.488 \times 10^{-7}$) and AUC (0.712 to 0.737; gain 0.0247). Compared with branch A, adjusted ORs for branches C and D were 2.61 and 4.83, respectively.

3.4 Mechanistic endpoint: AKI within 48 h

Among the 2,373 stays, creatinine follow-up within 48 h after $t_0$was available for 2,363 (99.6%). AKI48h differed significantly across branches (χ^2 test $p = 2.137 \times 10^{-7}$): A 22.5% (391/1739), B 21.3% (98/461), C 45.7% (48/105), and D 32.8% (19/58) (Table 5). After adjustment for age, sex, baseline creatinine, MAP, and 24 h total dose, adding branches still improved the AKI48h logistic model (LRT $p = 4.522 \times 10^{-5}$; AUC 0.601 to 0.612; gain 0.0114). Branch B had a lower adjusted odds of AKI48h compared with A (OR 0.525, 95% CI 0.379–0.726; $p = 9.924 \times 10^{-5}$).

Table 3: Cohort construction flow and sample sizes (MIMIC-IV v3.1).

Step	ICU stays (n_stays)	Subjects (n_subjects)	Admissions (n_hadm)
All ICU stays	94,458	65,366	85,242
Adult ICU stays ($\geq$ 18 years)	94,458	65,366	85,242
AHF ICD-9 ICU stays	5,899	4,150	5,080
AHF + IV loop diuretic within 24 h	2,825	2,233	2,645
After excluding ESRD/dialysis	2,695	2,140	2,523
After excluding sepsis (final)	2,373	1,889	2,223

Note: the ICU stay was the primary analysis unit; n_subjects and n_hadm are auxiliary counts.

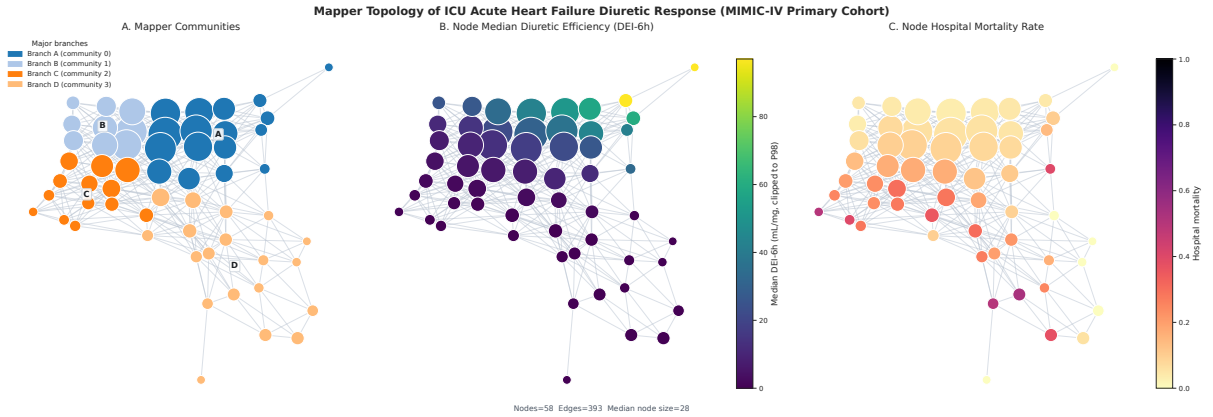


Fig. 1: Mapper graph and branch annotation (A–D). Panel A: discrete communities and major-branch labels; Panel B: node median DEI at 6 h (continuous scale); Panel C: node in-hospital mortality (continuous scale).

3.5 Sensitivity analyses: DEI denominator robustness and CVP inclusion

To mitigate denominator artifacts yielding implausibly high DEI, we quality-checked first-dose recordings: 48 stays had first furosemide-equivalent dose $<$ 5 mg and 83 had $<$ 10 mg. Under the original definition, DEI-6h had an extreme heavy tail (P99 258.99; max 27,600.00). Using a dose floor of 10 mg, excluding first dose $<$ 5 mg, or using the 24 h total dose as the denominator substantially reduced extremes (max 307.50 or 221.00; Table 6).

Given high CVP missingness ($\sim$80.7%), we repeated graph construction under two settings: complete removal of CVP versus retaining CVP with a missingness indicator. All five prespecified scenarios completed successfully, with best stability scores between 0.854 and 0.902 and 4–5 major branches, suggesting the core graph skeleton and risk gradient were not driven by extreme DEI values or the inclusion of CVP.

3.6 Dynamic response patterns: primary nonresponse and tachyphylaxis

Using piecewise DEI trajectories over 0–2 h, 2 h–6 h, and 6 h–12 h, we defined dynamic response patterns including primary nonresponse and tachyphylaxis (rapid attenuation). The distribution of primary nonresponse differed strikingly across branches (χ^2 test $p = 1.186 \times 10^{-104}$), with branch-level proportions of 0.232, 0.534, 1.000, and 1.000 for A/B/C/D. Tachyphylaxis also differed across branches ($p = 8.981 \times 10^{-8}$). Branch-level cumulative urine output and DEI trajectories are summarized in Figure 4.

Table 4: Major branches (A–D): sample size, response, and outcomes (anchored at t_0).

Branch	n	In-hospital mortality	DEI-6h (median)	Total dose in 24 h (median)	MAP (median)	Creatinine (median)
A	1747	7.0%	29.50	40.0	76.0	1.20
B	461	8.9%	12.21	231.7	77.0	2.00
C	105	29.5%	2.08	280.0	69.0	3.00
D	60	28.3%	0.00	75.0	73.0	2.00

Note: DEI is measured in mL/mg; total 24 h dose is the furosemide-equivalent dose (mg). Sensitivity analyses for DEI denominator robustness and CV

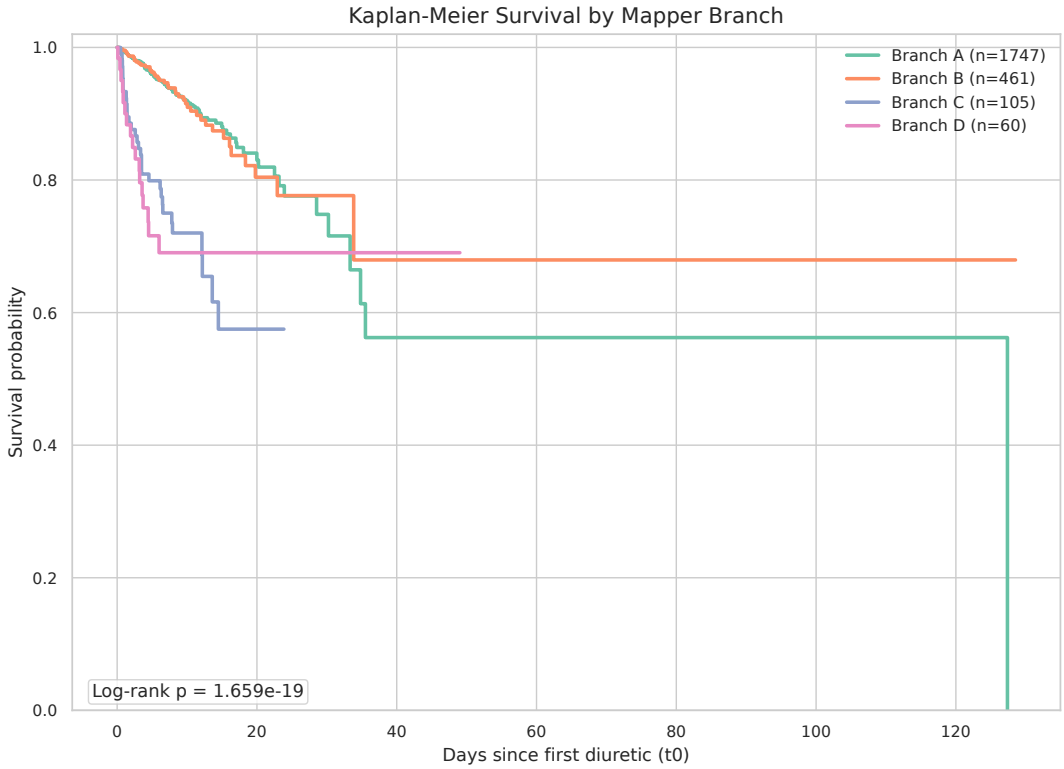


Fig. 2: Kaplan–Meier survival curves by branch (time zero at t_0).

3.7 External validation in eICU-CRD

In eICU-CRD v2.0, 4,438 ICU stays met the aligned eligibility criteria. Mapper recapitulated a comparable topology with 44 nodes and 207 edges (coverage 1.000) and high stability (mean Jaccard 0.965 ± 0.034; stability score 0.959), yielding three major branches. The major-branch structure and the response–risk gradient were consistent: the higher-DEI branch showed lower in-hospital mortality than the low-DEI branch (7.4% vs 11.4%), and mortality differed across branches (log-rank $p = 5.441 \times 10^{-4}$). Although effect sizes differed and time-to-event analyses used length of stay as a proxy time scale because precise event timestamps were not uniformly available in eICU-CRD, branch labels still provided incremental prognostic information beyond standard covariates (Cox LRT $p = 1.617 \times 10^{-2}$; logistic LRT $p = 1.235 \times 10^{-3}$; AUC gain 0.0091). AKI48h also differed across branches (chi-square $p = 1.174 \times 10^{-6}$), supporting cross-dataset consistency of the main conclusion.

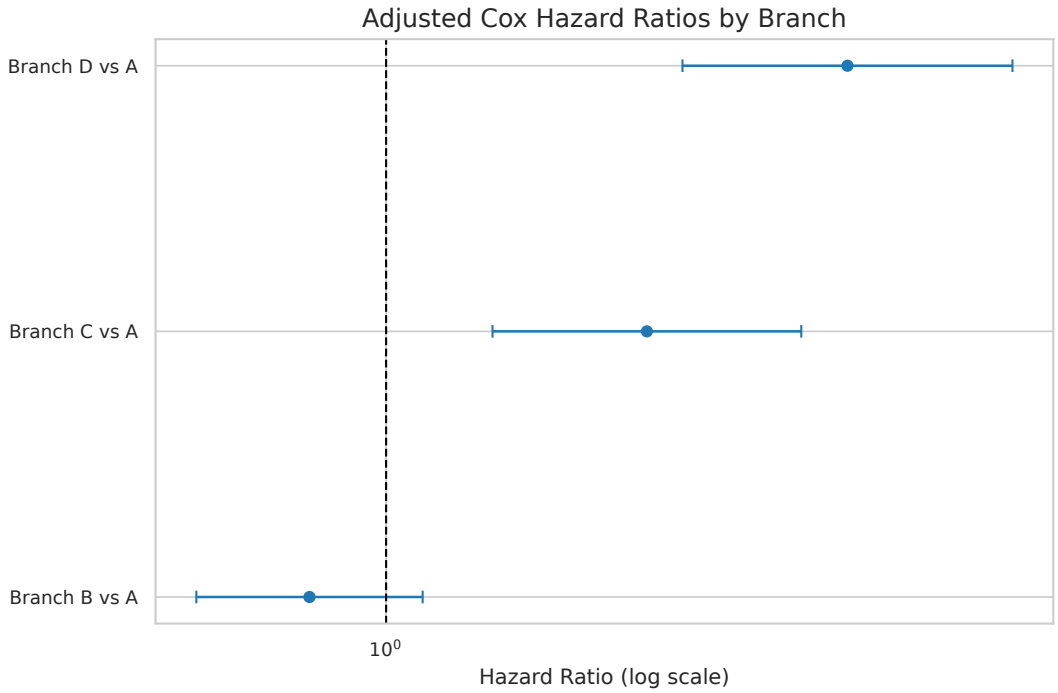


Fig. 3: Forest plot of branch effects in the multivariable Cox model adjusted for age, sex, creatinine, MAP, and 24 h dose.

Table 5: Incidence of AKI within 48 h after t_0(KDIGO creatinine proxy) by branch.

Branch	Follow-up n	AKI48h n (%)	Stage 2+ n (%)	Notes
A	1739	391 (22.5)	27 (1.6)	Reference
B	461	98 (21.3)	3 (0.7)	
C	105	48 (45.7)	1 (1.0)	
D	58	19 (32.8)	1 (1.7)	

Note: follow-up n denotes stays with at least one creatinine measurement between $t_0$and t_0+48 h. Percentages use follow-up n as the denominator. Stage 2+ is defined as maximum follow-up creatinine $\geq 2.0\times$ baseline.

4 Discussion

4.1 Key findings and clinical implications

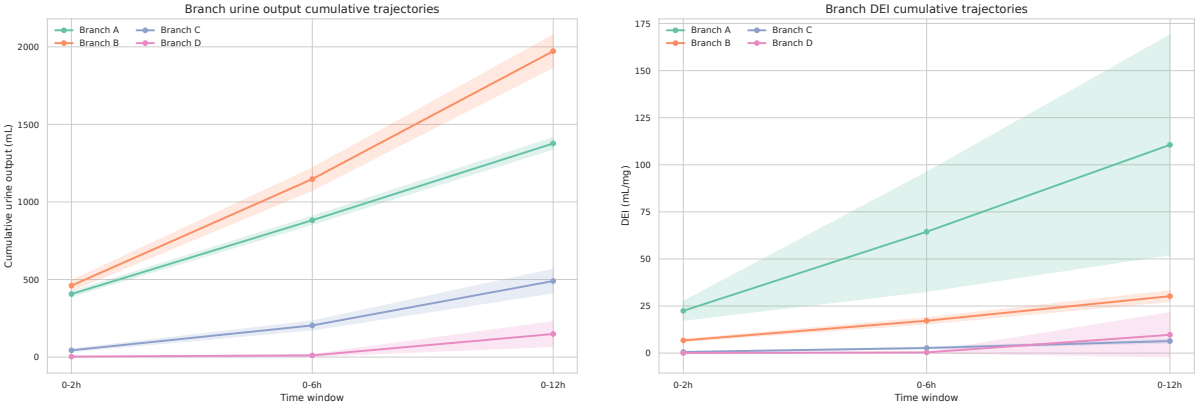
Anchoring feature extraction at the first ICU loop-diuretic dose (t_0), we constructed short-window urine-output and DEI dynamics and built an interpretable Mapper graph. We observed: **(1)** a robust graph skeleton with full coverage and high bootstrap stability; **(2)** a clear "response–renal function–outcome" gradient across major branches; **(3)** independent and incremental prognostic value of Mapper branches for in-hospital mortality beyond conventional covariates; and **(4)** pronounced heterogeneity of dynamic response patterns (primary nonresponse and tachyphylaxis) across branches, providing a structured complement to threshold-based definitions of diuretic resistance.

Beyond mortality, branches were also associated with AKI48h and provided incremental information after adjustment, suggesting that Mapper branches capture a high-dimensional joint structure of exposure, response, and physiologic

Table 6: Sensitivity analyses across DEI denominator robustification and CVP inclusion (Phase 4).

Scenario	n	CVP in Mapper	DEI denominator	DEI-6h P99	DEI-6h max
S0 Original (raw + CVP)	2373	Yes	Raw (first dose)	258.99	27600.00
S1 Floor10 + no CVP	2373	No	Dose floor 10 mg	149.42	307.50
S2 Floor10 + exclude $<$ 5 mg + no CVP	2325	No	Floor10 + exclude $<$ 5 mg	145.38	307.50
S3 Floor10 + total24h + no CVP	2373	No	24 h total-dose denominator	110.64	221.00
S4 Floor10 + CVP	2373	Yes	Dose floor 10 mg	149.42	307.50

Note: stability scores are from the best-performing network under each scenario (zero-filled mode). The number of major branches varied between 4 and was preserved.



(a) Cumulative urine output.

(b) Cumulative DEI.

Fig. 4: Dynamic response trajectories for branches A–D (mean and confidence intervals).

context rather than a single baseline creatinine value or a single urine-output threshold. This is consistent with recent EHR-based work suggesting that kidney-injury risk is heterogeneous and can be partitioned into clinically meaningful subphenotypes even within mild (stage-1) AKI [17]. Importantly, robustness checks across DEI denominator definitions and CVP inclusion/exclusion supported that the core skeleton and risk gradient were not artifacts of extreme DEI values or reliance on a highly missing monitoring variable.

From a clinical-interpretation perspective, branch C combined low DEI, higher dose exposure, higher baseline creatinine/BUN, and the highest mortality—a pattern consistent with severe cardiorenal syndrome and "true" resistance that may warrant early escalation and diuretic potentiation strategies [5, 6, 18, 19]. Branch D showed near-zero early DEI and enrichment of primary nonresponse, yet baseline kidney function and dose exposure were not uniformly worst, suggesting a mixed pathway that may include delayed responders, documentation sparsity, or unmeasured treatment differences. Branch B appeared to represent a dose-escalation transition zone with intermediate efficiency but high 24 h dose and higher renal burden. Recent comparative work on diuretic regimens underscores that apparent "efficacy" can vary across congestion states and patient contexts [20]. Smaller branches (C and D) require validation in larger multi-center cohorts to assess transportability and mechanistic interpretability.

In addition to urine output, urinary sodium has been proposed as an early objective signal of diuretic response in AHF and a potential trigger for escalation; its relationship with renal function and its real-world uptake remain active areas of investigation [4, 21, 22].

4.2 Methodological considerations: transparency and robustness

We emphasize a transparent end-to-end workflow: code-based extraction and variable construction; explicit t_0-anchored time windows; two-stage parameter search with bootstrap stability quantification; branch annotation and layered outcome modeling (unadjusted, adjusted, and incremental value); and prespecified sensitivity analyses addressing denominator artifacts and high-missingness monitoring variables, complemented by a mechanistic kidney-injury endpoint (AKI48h). This design aimed to reduce the influence of parameter tuning, missingness structure, and recording artifacts on the derived topological skeleton and the main conclusions.

More broadly, recent EHR subphenotyping work has highlighted the importance of stability and transportability when cluster structures are derived from high-dimensional clinical trajectories [23–25]. Our bootstrap co-membership evaluation was intended to make the derived topology more reproducible and easier to validate in future multi-center cohorts.

4.3 Limitations and future work

Several limitations warrant consideration. First, loop-diuretic dosing and DEI remain subject to residual uncertainty: although robustness checks supported structural stability, first-dose recordings may not fully represent true early exposure under continuous infusions or fragmented documentation; future work should integrate short-window cumulative dosing (e.g., 0–2 h and 0–6 h) and infusion-rate information to better approximate pharmacologic exposure. Second, AKI48h used a creatinine proxy and did not use the KDIGO urine-output criterion to avoid overlap with response features, which may underestimate AKI incidence and severity; future work should explore outcome definitions that remain disentangled from the response features (or incorporate RRT/CRRT and net fluid balance). Third, highly missing monitoring variables (CVP/NT-proBNP) can introduce explainability bias because "being measured" may itself reflect severity and monitoring strategy; richer intervention and monitoring covariates are needed. Fourth, an ICD-9-based AHF definition limits generalizability across centers and coding practices; more transferable phenotype definitions should be explored. Finally, residual confounding remains possible; future analyses should incorporate broader confounder control (comorbidities, vasoactive drugs, ventilation, baseline fluid balance, RRT) and robustness checks (propensity methods, alternative endpoints, and time-varying covariates).

5 Conclusion

A t_0-anchored framework combining dynamic urine-output response features with an interpretable Mapper topology can identify stable diuretic-response subtypes in ICU patients with AHF. These topological branches provide independent and incremental prognostic information for in-hospital mortality and are associated with early kidney injury (AKI48h), offering a data-driven path from threshold-based "resistance" toward structured response-spectrum phenotyping.

Supplementary information. Supplementary material is available and provides detailed variable definitions, parameter-search results, and additional robustness analyses.

Acknowledgements. We thank PhysioNet and the MIT Laboratory for Computational Physiology for providing access to high-quality open critical care data resources.

Statements and Declarations

Funding: Not applicable.
Competing interests: The author declares no competing interests.
Ethics approval and consent to participate: MIMIC-IV and eICU-CRD are de-identified databases. For MIMIC-IV, the requirement for individual informed consent was waived by the institutional review board of Beth Israel Deaconess Medical Center. This study used only de-identified data under the respective data use agreements.
Consent for publication: Not applicable.
Data availability: MIMIC-IV (https://physionet.org/content/mimiciv/) and eICU-CRD (https://physionet.org/content/eicu-crd/) are available via PhysioNet to credentialed users

who complete the required training and data use agreements.
Materials availability: Not applicable.
Code availability: Code is available from the corresponding author upon reasonable request.
Author contributions: Jiacheng Tian: Conceptualization, Methodology, Formal analysis, Visualization, Writing–original draft, Writing–review and editing.

References

[1] McDonagh TA, Metra M, Adamo M, ESC Scientific Document Group. 2021 ESC Guidelines for the diagnosis and treatment of acute and chronic heart failure. Eur Heart J. 2021;42(36):3599–3726. https://doi.org/10.1093/eurheartj/ehab368.

[2] ter Maaten JM, Dunning AM, Valente MAE, Damman K, Voors AA. Diuretic response in acute heart failure–pathophysiology, evaluation, and therapy. Nat Rev Cardiol. 2015;12(3):184–192. https://doi.org/10.1038/nrcardio.2014.215.

[3] Segar MW, Khan MS, Patel KV, Butler J, Ravichandran AK, Walsh MN, et al. A Phenomapping Tool and Clinical Score to Identify Low Diuretic Efficiency in Acute Decompensated Heart Failure. JACC Heart Fail. 2024;12(3):508–520. https://doi.org/10.1016/j.jchf.2023.09.029.

[4] Meekers E, Dauw J, ter Maaten JM, Martens P, Nijst P, Verbrugge FH, et al. Urinary Sodium Analysis: The Key to Effective Diuretic Titration? European Journal of Heart Failure Expert Consensus Document. Eur J Heart Fail. 2025;27(6):940–949. https://doi.org/10.1002/ejhf.3632.

[5] Siddiqi TJ, Packer M, Ezekowitz JA, Fonarow GC, Greene SJ, Kittleson M, et al. Diuretic Potentiation Strategies in Acute Heart Failure. JACC Heart Fail. 2025;13(1):14–27. https://doi.org/10.1016/j.jchf.2024.09.017.

[6] Fioretti F, Praderio A, Nodari S, Metra M, Butler J. Combination Diuretic Therapy in Acute Heart Failure: A Systematic Review and Meta-Analysis. Eur J Heart Fail. 2025;27(12):3096–3110. https://doi.org/10.1002/ejhf.70094.

[7] Jentzer JC, Reddy YNV, Soussi S, Crespo-Diaz R, Patel PC, Lawler PR, et al. Unsupervised Machine Learning to Identify Subphenotypes Among Cardiac Intensive Care Unit Patients with Heart Failure. ESC Heart Fail. 2024;11(6):4242–4256. https://doi.org/10.1002/ehf2.15027.

[8] Singh G, Mémoli F, Carlsson G. Topological Methods for the Analysis of High Dimensional Data Sets and 3D Object Recognition. In: Eurographics Symposium on Point-Based Graphics; 2007. .

[9] Tauzin G, Lupo U, Tunstall L, et al. giotto-tda: A Topological Data Analysis Toolkit for Machine Learning and Data Exploration. J Mach Learn Res. 2021;22(39):1–6.

[10] Platt D, Bose A, Rhrissorrakrai K, Levovitz C, Parida L. Epidemiological topology data analysis links severe COVID-19 to RAAS and hyperlipidemia associated metabolic syndrome conditions. Bioinformatics. 2024;40(Suppl. 1):i199–i207. https://doi.org/10.1093/bioinformatics/btae235.

[11] Johnson AEW, Bulgarelli L, Shen L, et al. MIMIC-IV, a freely accessible electronic health record dataset. Sci Data. 2023;10(1):1. https://doi.org/10.1038/s41597-022-01899-x.

[12] Pollard TJ, Johnson AEW, Raffa JD, Celi LA, Mark RG, Badawi O. The eICU Collaborative Research Database, a freely available multi-center database for critical care research. Sci Data. 2018;5(1):180178. https://doi.org/10.1038/sdata.2018.178.

[13] Pollard TJ, Johnson AEW, Raffa J, Badawi O.: The eICU Collaborative Research Database. physionet.org. Available from: https://doi.org/10.13026/C2WM1R.

[14] van Buuren S, Groothuis-Oudshoorn K. mice: Multivariate Imputation by Chained Equations in R. J Stat Softw. 2011;45(3):1–67. https://doi.org/10.18637/jss.v045.i03.

[15] Ester M, Kriegel HP, Sander J, Xu X. A density-based algorithm for discovering clusters in large spatial databases with noise. In: Proceedings of the Second International Conference on Knowledge Discovery and Data Mining (KDD); 1996. p. 226–231.

[16] Group KAKIW. KDIGO Clinical Practice Guideline for Acute Kidney Injury. Kidney Int Suppl. 2012;2(1):1–138.

[17] Li D, Chan HY, Yu ASL, Kellum JA, Fuhrman DY, Chrischilles EA, et al. Clustering analysis of multi-site electronic health records reveals distinct subphenotypes in stage-1 acute kidney injury. Commun Med. 2025;5(1):274. https://doi.org/10.1038/s43856-025-00993-6.

[18] Lo KB, Nohria A. Diuretic strategies in acute decompensated heart failure. Heart Fail Rev. 2024;30(2):417–430. https://doi.org/10.1007/s10741-024-10473-z.

[19] Pandey A, Segar MW, Keshvani N, Ll 'acer P, Casado J, Morales-Rull JL, et al. Diuretic Resistance and the Efficacy of Hydrochlorothiazide in Acute Decompensated Heart Failure: A Post-Hoc Analysis of the CLOROTIC Trial. Eur J Heart Fail. 2025;27(12):3142–3150. https://doi.org/10.1002/ejhf.70002.

[20] Abbo AR, Gruber A, Volis I, Aronson D, Girerd N, Kristensen SL, et al. Diuresis Efficacy in Ambulatory Congested Heart Failure Patients. JACC Heart Fail. 2024;12(8):1396–1405. https://doi.org/10.1016/j.jchf.2024.04.014.

[21] Caravaca Pérez P, Fernández-Herrero I, Broseta JJ, Ibarra-Márquez N, Blázquez-Bermejo Z, López-Azor JC, et al. Impact of natriuresis on worsening renal function during episodes of acute heart failure. Rev Esp Cardiol (Engl Ed). 2025;78(3):196–205. https://doi.org/10.1016/j.rec.2024.07.006.

[22] Cobo Marcos M, Trullàs JC, Perez-Silvestre J, Miró Ò, Quiroga B, Mirabet S, et al. Urinary sodium to guide diuretic therapy in acute heart failure: results of a national survey. ESC Heart Failure. 2026;13(1):xvag006. https://doi.org/10.1093/eschf/xvag006.

[23] Mariam A, Javidi H, Zabor EC, Zhao R, Radivoyevitch T, Rotroff DM. Unsupervised clustering of longitudinal clinical measurements in electronic health records. PLOS Digit Health. 2024;3(10):e0000628. https://doi.org/10.1371/journal.pdig.0000628.

[24] Qiu J, Hu Y, Li L, Erzurumluoglu AM, Braenne I, Whitehurst C, et al. Deep representation learning for clustering longitudinal survival data from electronic health records. Nat Commun. 2025;16(1):2534. https://doi.org/10.1038/s41467-025-56625-z.

[25] Ferris JK, Fiedeldey LK, Kim B, Clemens F, Irvine MA, Hosseini SH, et al. A systematic review and meta-analysis of disease clusters in multimorbidity. Nat Commun. 2025;17(1):634. https://doi.org/10.1038/s41467-025-67372-6.

Supplementary Files

This is a list of supplementary files associated with this preprint. Click to download.

- supplement.pdf